MAGNETIC FIELD CALCULATION IN PERMANENT MAGNET MOTORS WITH ROTOR ECCENTRICITY : WITHOUT SLOTTING EFFECT

Ungtae Kim and Dennis K. Lieu

Electro-Mechanical Design Laboratory

Department of Mechanical Engineering

University of California at Berkeley

Berkeley, CA 94720

ABSTRACT

An analytical technique for predicting the instantaneous magnetic field distribution in the air gap region of permanent magnet motors with rotor eccentricity is developed. The governing equations and the associated boundary conditions are formulated and solved by a perturbation method. The predicted solutions are verified by the results of a corresponding finite element analysis. The results show the effectiveness of using the perturbation method for this eccentric field calculation. According to this study, the additional flux density due to the rotor eccentricity is proportional to the amount of the eccentricity in a small range and has a quite different distribution from the normal flux density without the rotor eccentricity. Accordingly, the rotor eccentricity may cause undesirable effects on brushless permanent magnet motors.

I. INTRODUCTION

The spindle motor is one of the most important elements of a disk drive and, on the other hand, acts as a frequent source of vibration induced by magnet forces or defects of its structural components. It has a profound effect on the performance and the capacity of a disk drive through its configuration, operating speed, runouts, and resonances. Therefore a great number of efforts have been made to achieve technological innovations and market competitiveness. Among them, size reduction, spindle speed increase, and cost reduction have been the main concerns[1]. As the disk size is reduced, the spindle speed must increase for a given maximum bit density and media data rate. Thus, the high speed use will continue to improve disk drive performance. However, this increase in speed will place a greater emphasis on the spindle motor and bearing design. Much more precise manufacturing process is also needed. A great number of papers have been published on the spindle motor and bearing design in relation to higher speed effects, whereas few literatures are found which examine the performance and the dynamic effects of the spindle motor caused by manufacturing imprecisions. One of many concerns is the rotor eccentricity which may result from unavoidable errors or working allowances from manufacturing processes. For example, ball bearing defects such as excessive clearance and waviness may create eccentricity problems and so do resonant vibrations of the rotor and bearing system in the hard disk drive. In fluid bearings which will be extensively used for high speed spindles, eccentricity occurs inherently due to the unbalanced distribution of pressure. The rotor eccentricity may yield problems in magnetic and dynamic aspects causing additional vibration, noise, and torque pulsation. It is believed to either directly or indirectly affect the track following error in the disk drive. Thus it is necessary to start

studying the magnetic field analysis produced by the rotor eccentricity in permanent magnet motors rotating in high speed.

Eccentricity has long been studied with an emphasis on the calculation of the air gap field [2] and its effect on the unbalanced magnet pull (UMP)[3]. Belmans et al has analyzed the UMP and its relationship between the stability of an induction machine shaft with eccentricity [4]. Other authors have examined the presence of unique signature patterns in the current and vibration spectra which can show characteristics of eccentricity [5] and methods to detect the eccentricity [6]. Many studies concerning on the eccentricity effects on induction motors have been reported, but few publications have appeared regarding permanent magnet synchronous or brushless DC motors. Zhu and Howe have referred to the effect of eccentricity on additional acoustic noise and vibration source in brushless permanent magnet motors [7]. Chao et al has also mentioned it as a possible torque pulsation source but did not elaborate on the details [8]. All of the authors mentioned above have handled the eccentricity problem by using relative permeance functions, considering only the fact that the air gap permeance varies inversely as the air gap length. But using the permeance functions is an indirect way to describe the magnetic field due to eccentricity and may lead to a poor understanding. One dimensional permeance functions can only explain the overall behavior of the eccentric magnetic field at the stator outer surface but can not describe details induced by the pulsating magnet forces and boundary effects due to the rotor eccentricity. Most papers using the permeance functions for the eccentric field calculation could not include the whirling phenomenon of the rotor effectively. More rigorous explanation in the field is needed for other applications such as

rotor dynamic problems excited by the magnetic field of a motor supported by fluid film bearings.

In this paper, a direct analysis of the magnetic field induced by the rotor eccentricity in permanent magnet motors is explained. The governing equations and the associated boundary conditions are formulated for an external rotor motor in two dimensions by a perturbation method. Static and dynamic eccentricities are considered. Analytical results are compared with those of a corresponding finite element method. This work can be used as the basis for future practical applications regarding the rotor eccentricity of other motors or magnetic bearings.

II. MAGNETIC FIELD INDUCED BY ROTOR ECCENTRICITY

A. Problem Description

This paper presents an analytical method for the magnetic field produced by a permanent magnet motor with rotor eccentricity. Fig. 1 shows a schematic geometry of a motor including the geometric notations which will be used in the following analysis. The magnetic field is produced by an external rotor which rotates with the angular velocity of ω about the axis O_r and whirls around the axis O_s with the angular velocity of Ω. The radial distance between the two axes is defined as the eccentricity of the rotor and is denoted by

$$\varepsilon = e \cdot g \tag{1}$$

where e is the eccentricity ratio and g is the nominal air gap length. Note that the eccentricity ratio e, has the following limits.

$$0 \le e \le 1 \tag{2}$$

The X-Y coordinate system is fixed to the center of the stator O_s, whereas the x-y coordinate system is attached to the center of the rotor O_r and rotates with the same angular velocity as the rotor. The x'-y' coordinate system does not rotate and expresses the relative position of the rotor with respect to the stator position by the quantities ε and ϕ, the whirling position at an instant which can be expressed as Ωt without the loss of generality. The rotor eccentricity in a motor can be divided into three types: static eccentricity, dynamic eccentricity, and their combination. Static eccentricity with which the rotor is displaced from the stator center but is still turning upon its own axis O_r, can be modeled by assuming ε and ϕ as constants. Dynamic eccentricity with which the rotor is turning around the stator, can also be treated by considering them as functions of the time and the position, which can be determined by solving the associated rotor dynamic problem [9].

In order to limit the mathematical efforts and to gain physical insight regarding the problem, the following assumptions are made in this study. First, both the rotor and stator surfaces are perfect cylinders, and the axis of the rotor is parallel to the axis of the stator, i.e., only translatory eccentricity is considered, which still renders the problem to be two dimensional. Second, the effects of slotting are neglected. Third, the permeability of the rotor and the stator back iron is infinite. And last, the eddy current and the saturation effects are neglected.

B. Coordinate Transformations of Two Reference Frames

An arbitrary point P in the air gap or the permanent magnet region in Fig. 2 can be expressed in terms of either r-θ or ξ-ψ coordinates, which can be transformed into each other as follows.

$$\xi = r - \varepsilon \cos(\theta - \phi) + O(\varepsilon^2) \tag{3a}$$

$$\psi = \theta - \omega t + \frac{\varepsilon}{r} \sin(\theta - \phi) + O(\varepsilon^2) \tag{3b}$$

Throughout the following analysis, only linear components in perturbation equations are retained, which is not unusual for most perturbation analyses. The detailed derivation of the transformation equations is given in Appendix 1.

C. Magnetic Field Equation

A quasi-static field is a dynamic field in which the effects of inertia can be neglected. In a magnetic field, a quasi-static condition occurs when the propagation time for an electromagnetic wave within a device is small compared to the characteristic time associated with the motion of the device. Most electromechanical devices, including permanent magnet motors, are characterized in terms of quasi-static magnetic fields. The magnetic field that is produced as the rotor rotates can be assumed as a series of magneto-static fields, which helps to transform the governing equations into the quasi-Poisson type equations. In this section, a perturbation formulation is explained for modeling the quasi-static magnetic field produced by the eccentric rotor. The perturbation analysis appears plausible, since the rotor eccentricity is usually small in comparison to the air gap length.

The governing equations and the associated boundary conditions are formulated in the fixed coordinate system, which can easily reveal the perturbing effects of the magnets and

their boundaries. However, this procedure yields some mathematical deficiencies. Firstly, an undesirable form of an exciting forcing term occurs in the governing equations which can not be handled easily. Secondly, the Poisson equations are to be solved by a series expansion method, in which the series need to be differentiated twice. This may lead to a problem of uniform convergence of the solutions despite the small perturbation. Thirdly, more complicated boundary conditions are required, since the number of asymmetries increases in the fixed coordinate system. Thus, for pure mathematical reasons, the field equations are formulated and solved in the moving coordinate system and are transformed into those in the fixed coordinate system by the transformation equations (3a,b). This is acceptable in a quasi-static system if the whirling speed Ω is constant and the moving coordinate system is considered as an initial reference frame. In this case, the governing equations and the associated boundary conditions are invariant in terms of the moving coordinates [10].

D. Derivation of the Governing Equations and the Boundary Conditions

In this section, general equations of a magnetic field are derived. The field vectors $\vec{B}$ and $\vec{H}$ are written as

$$\vec{B}_1 = \mu_0 \vec{H}_1 \tag{4}$$

$$\vec{B}_2 = \mu_m \vec{H}_2 + \mu_0 \vec{M} \tag{5}$$

where the subscripts 1 and 2 denote the air gap and the permanent magnet region, respectively; $\vec{M}$ is the residual magnetization vector of magnitude B_r/μ_0 , where B_r is the remanence. The equation for the recoil permeability of the permanent magnets is given

by $\mu_m = \mu_0 \mu_r$, where μ_r is the relative recoil permeability. The vector $\vec{M}$ can be expressed by a Fourier series form as previously reported by Zhu et al [11],

Introducing the scalar magnetic potential Φ defining

$$\vec{H} = -\nabla \Phi \tag{6}$$

makes the coupled Maxwell equations into Poisson type equations in the respective regions where there is no current source. The governing equations are, then,

$$\nabla^2 \Phi_1 = 0 \tag{7a}$$

$$\nabla^2 \Phi_2 = \frac{1}{\mu_r} \nabla \cdot \vec{M} \tag{7b}$$

In polar coordinates originating from the moving (*x*-*y*) coordinate system, the above equations are expressed as

$$\frac{\partial^2 \Phi_1}{\partial \xi^2} + \frac{1}{\xi} \frac{\partial \Phi_1}{\partial \psi} + \frac{1}{\xi^2} \frac{\partial^2 \Phi_1}{\partial \psi^2} = 0 \tag{8a}$$

$$\frac{\partial^2 \Phi_2}{\partial \xi^2} + \frac{1}{\xi} \frac{\partial \Phi_2}{\partial \psi} + \frac{1}{\xi^2} \frac{\partial^2 \Phi_2}{\partial \psi^2} = \frac{1}{\mu_r} \frac{M_\xi}{\xi} \tag{8b}$$

where M_ξ is the ξ-direction component of the magnetization vector $\vec{M}$ given by

$$M_\xi = \sum_{n=1,3,5\cdots}^{\infty} M_n \cos(np\psi) \tag{9}$$

Here M_n is again given by

$$M_n = 2\left(\frac{B_r}{\mu_0}\right) \alpha_p \frac{\sin \frac{n\pi\alpha_p}{2}}{\frac{n\pi\alpha_p}{2}} \tag{10}$$

where *p* is the number of the magnet pole pairs, and α_p is the ratio of the pole-arc to pole-pitch of the magnets.

The field intensity vectors are related to the magnetic potential functions by

$$H_{\xi,i} = -\frac{\partial \Phi_i}{\partial \xi} \tag{11a}$$

$$H_{\psi,i} = -\frac{1}{\xi}\frac{\partial \Phi_i}{\partial \psi} \tag{11b}$$

where $i = 1$ and $i = 2$ again for the air gap and the permanent magnet region, respectively.

The boundary conditions are described by

$$\vec{n} \times \left\| \vec{H} \right\| = 0 \tag{12a}$$

$$\vec{n} \bullet \left\| \vec{B} \right\| = 0 \tag{12b}$$

where $\vec{n}$ is the normal vector along the associated boundary and $\|\cdot\|$ represents the amount by which a value differs on the two sides of the boundary. Note that the normal vector $\vec{n}$ is a function of the eccentricity components ε and ϕ, as well as the instantaneous rotational position of the rotor, ωt. It can also be expressed in the moving coordinate system as described in the next section.

Magnetic potential equations (8a) and (8b) together with the boundary conditions describe the magnetic flow from the north poles to the south poles of the magnets through the eccentric air gap region. Note that the rotor eccentricity effect only occurs on the boundary of the stator in the moving coordinate system, which makes mathematics simpler.

For the stator boundary described by

$$f(\xi,\psi,\varepsilon) = \xi + \varepsilon\cos(\psi + \omega t - \phi) - R_s + O(\varepsilon^2) = 0 \tag{13}$$

the normal vector is

$$\vec{n}(\xi,\psi,\varepsilon) = \frac{\nabla f}{|\nabla f|} = \hat{e}_\xi - \frac{\varepsilon}{\xi}\sin(\psi + \omega t - \phi)\hat{e}_\psi + O(\varepsilon^2) \tag{14}$$

where $\hat{e}_\xi$ and $\hat{e}_\psi$ are the unit vectors ascribed to the moving coordinates. Again only the terms up to the first order will be retained in the following analysis, and the perturbation order symbol will be omitted for simplicity.

The boundary condition along the surface of the stator for an external rotor motor is represented by

$$\vec{n} \times \left(H_{\xi,1} \hat{e}_\xi + H_{\psi,1} \hat{e}_\psi \right) = 0 \tag{15}$$

After some vector calculations, equation(15) is written explicitly as

$$H_{\psi,1}(\xi,\psi,\varepsilon) + \frac{\varepsilon}{\xi} \sin(\psi + \omega t - \phi) H_{\xi,1}(\xi,\psi,\varepsilon) \Big|_{\xi = R_s - \varepsilon \cos(\psi + \omega t - \phi)} = 0 \tag{16}$$

The other boundary conditions are obtained by

$$H_{\psi,2}(\xi,\psi,\varepsilon)\Big|_{\xi=R_r} = 0 \tag{17}$$

$$B_{\xi,1}(\xi,\psi,\varepsilon)\Big|_{\xi=R_m} = B_{\xi,2}(\xi,\psi,\varepsilon)\Big|_{\xi=R_m} \tag{18}$$

$$H_{\psi,1}(\xi,\psi,\varepsilon)\Big|_{\xi=R_m} = H_{\psi,2}(\xi,\psi,\varepsilon)\Big|_{\xi=R_m} \tag{19}$$

where the radii of the magnets and the rotor are defined by $R_m = R_s + g$ and $R_r = R_s + g + h_m$ for an external rotor motor, h_m being the radial thickness of the magnets.

By considering the boundary condition (16), regular perturbation expansions of the moving coordinates are proposed in the following forms.

$$\Phi_1(\xi,\psi,\varepsilon) = \Phi_1^{(0)}(\xi,\psi) + \varepsilon \Phi_1^{(1)}(\xi,\psi) + \cdots \tag{20a}$$

$$\Phi_2(\xi,\psi,\varepsilon) = \Phi_2^{(0)}(\xi,\psi) + \varepsilon \Phi_2^{(1)}(\xi,\psi) + \cdots \tag{20b}$$

The field intensity vectors in the concerning regions are thus represented by

$$H_{\xi,i}(\xi,\psi,\varepsilon)=-\frac{\partial \Phi_i^{(0)}(\xi,\psi)}{\partial \xi}-\varepsilon\frac{\partial \Phi_i^{(1)}(\xi,\psi)}{\partial \xi}-\cdots \tag{21a}$$

$$H_{\psi,i}(\xi,\psi,\varepsilon)=-\frac{1}{\xi}\frac{\partial \Phi_i^{(0)}(\xi,\psi)}{\partial \psi}-\varepsilon\frac{1}{\xi}\frac{\partial \Phi_i^{(1)}(\xi,\psi)}{\partial \psi}-\cdots \tag{21b}$$

where again the subscript i implies 1 or 2 for the air gap and the permanent magnet region, respectively.

By substituting equations (21a,b) into equation (16) and a Taylor series expansion about the nominal radius of the stator R_s, groups of the governing equations and the corresponding boundary conditions are thus derived.

The zeroth-order governing equations are

$$\frac{\partial^2 \Phi_1^{(0)}}{\partial \xi^2}+\frac{1}{\xi}\frac{\partial \Phi_1^{(0)}}{\partial \xi}+\frac{1}{\xi^2}\frac{\partial^2 \Phi_1^{(0)}}{\partial \psi^2}=0 \tag{22a}$$

$$\frac{\partial^2 \Phi_2^{(0)}}{\partial \xi^2}+\frac{1}{\xi}\frac{\partial \Phi_2^{(0)}}{\partial \xi}+\frac{1}{\xi^2}\frac{\partial^2 \Phi_2^{(0)}}{\partial \psi^2}=\frac{1}{\mu_r}\frac{M_\xi}{\xi} \tag{22b}$$

and the zeroth-order boundary conditions are

$$-\frac{1}{R_s}\frac{\partial \Phi_1^{(0)}(\xi,\psi)}{\partial \psi}\bigg|_{\xi=R_s}=0 \tag{23}$$

$$-\frac{1}{R_r}\frac{\partial \Phi_2^{(0)}(\xi,\psi)}{\partial \psi}\bigg|_{\xi=R_r}=0 \tag{24}$$

$$-\mu_0\frac{\partial \Phi_1^{(0)}(\xi,\psi)}{\partial \xi}\bigg|_{\xi=R_m}=-\mu_0\mu_r\frac{\partial \Phi_2^{(0)}(\xi,\psi)}{\partial \xi}\bigg|_{\xi=R_m}+\mu_0 M_\xi\Big|_{\xi=R_m} \tag{25}$$

$$-\frac{1}{R_m}\frac{\partial \Phi_1^{(0)}(\xi,\psi)}{\partial \psi}\bigg|_{\xi=R_m}=-\frac{1}{R_m}\frac{\partial \Phi_2^{(0)}(\xi,\psi)}{\partial \psi}\bigg|_{\xi=R_m} \tag{26}$$

The first-order governing equations are

$$\frac{\partial^2 \Phi_1^{(1)}}{\partial \xi^2} + \frac{1}{\xi}\frac{\partial \Phi_1^{(1)}}{\partial \psi} + \frac{1}{\xi^2}\frac{\partial^2 \Phi_1^{(1)}}{\partial \psi^2} = 0 \tag{27a}$$

$$\frac{\partial^2 \Phi_2^{(1)}}{\partial \xi^2} + \frac{1}{\xi}\frac{\partial \Phi_2^{(1)}}{\partial \psi} + \frac{1}{\xi^2}\frac{\partial^2 \Phi_2^{(1)}}{\partial \psi^2} = 0 \tag{27b}$$

Note that equation (27b) does not have an exciting forcing term unlike in equation (22b).

The first-order boundary conditions are

$$\begin{aligned} \frac{1}{R_s}\frac{\partial \Phi_1^{(1)}(\xi,\psi)}{\partial \psi}\bigg|_{\xi=R_s} &= -\frac{1}{R_s^2}\frac{\partial \Phi_1^{(0)}(\xi,\psi)}{\partial \psi}\bigg|_{\xi=R_s} \cos(\psi+\omega t-\phi) \\ &\quad + \frac{1}{R_s}\frac{\partial^2 \Phi_1^{(0)}(\xi,\psi)}{\partial \xi \partial \psi}\bigg|_{\xi=R_s} \cos(\psi+\omega t-\phi) \\ &\quad - \frac{1}{R_s}\frac{\partial \Phi_1^{(0)}(\xi,\psi)}{\partial \xi}\bigg|_{\xi=R_s} \sin(\psi+\omega t-\phi) \end{aligned} \tag{28}$$

$$-\frac{1}{R_r}\frac{\partial \Phi_2^{(1)}(\xi,\psi)}{\partial \psi}\bigg|_{\xi=R_r} = 0 \tag{29}$$

$$-\mu_0 \frac{\partial \Phi_1^{(1)}(\xi,\psi)}{\partial \xi}\bigg|_{\xi=R_m} = -\mu_0\mu_r \frac{\partial \Phi_2^{(1)}(\xi,\psi)}{\partial \xi}\bigg|_{\xi=R_m} \tag{30}$$

$$-\frac{1}{R_m}\frac{\partial \Phi_1^{(1)}(\xi,\psi)}{\partial \psi}\bigg|_{\xi=R_m} = -\frac{1}{R_m}\frac{\partial \Phi_2^{(1)}(\xi,\psi)}{\partial \psi}\bigg|_{\xi=R_m} \tag{31}$$

A sequence of problems with the unperturbed boundary conditions can be solved. For equations (22a,b) and the boundary conditions (23-26), the general solutions of the zeroth-order for the scalar magnetic potential distribution in the air gap and the magnets are obtained by considering the periodicity of the field.

$$\Phi_1^{(0)}(\xi,\psi) = \sum_{n=1,3,5\cdots}^{\infty} \left(A_{1n}^0 \xi^{np} + B_{1n}^0 \xi^{-np}\right)\cos np\psi \tag{32}$$

$$\Phi_2^{(0)}(\xi,\psi) = \sum_{n=1,3,5\cdots}^{\infty}\left(A_{2n}^{0}\xi^{np} + B_{2n}^{0}\xi^{-np}\right)\cos np\psi + \sum_{n=1,3,5\cdots}^{\infty}\frac{\xi\cdot M_n}{\mu_r\left[1-(np)^2\right]}\cos np\psi \tag{33}$$

The arbitrary constants A^0_{1n}, B^0_{1n}, A^0_{2n} , and B^0_{2n} are easily obtained by substituting the boundary conditions. A detailed procedure for obtaining the general solution is described in the paper by Zhu et al [11].

The zeroth-order solutions for the flux density distribution in the air gap region are given in the paper by Zhu et al [11] as

$$B_{\xi,1}^{(0)}(\xi,\psi) = \sum_{n=1,3,5\cdots}^{\infty}\frac{\mu_0 M_n}{\mu_r}\frac{np}{(np)^2-1}R_m^{-(np-1)}$$

$$\cdot\left\{\frac{(np-1)R_m^{2np} + 2R_r^{np+1}R_m^{np-1} - (np+1)R_r^{2np}}{\frac{\mu_r+1}{\mu_r}\left[R_s^{2np}-R_r^{2np}\right] - \frac{\mu_r-1}{\mu_r}\left[R_m^{2np} - R_s^{2np}\left(R_r/R_m\right)^{2np}\right]}\right\}$$

$$\cdot\left[\xi^{np-1} + R_s^{2np}\xi^{-(np+1)}\right]\cos(np\psi) \tag{34}$$

$$B_{\psi,1}^{(0)}(\xi,\psi) = \sum_{n=1,3,5\cdots}^{\infty} -\frac{\mu_0 M_n}{\mu_r}\frac{np}{(np)^2-1}R_m^{-(np-1)}$$

$$\cdot\left\{\frac{(np-1)R_m^{2np} + 2R_r^{np+1}R_m^{np-1} - (np+1)R_r^{2np}}{\frac{\mu_r+1}{\mu_r}\left[R_s^{2np}-R_r^{2np}\right] - \frac{\mu_r-1}{\mu_r}\left[R_m^{2np} - R_s^{2np}\left(R_r/R_m\right)^{2np}\right]}\right\}$$

$$\cdot\left[\xi^{np-1} - R_s^{2np}\xi^{-(np+1)}\right]\sin(np\psi) \tag{35}$$

The following solutions for the first-order governing equations (27a,b) are proposed by considering the boundary conditions and the periodicity of the field in the ξ-ψ coordinates.

$$\Phi_1^{(1)}(\xi,\psi) = \sum_{n=1,3,5\cdots}^{\infty}\left\{\left(A_{1n}^{1}\xi^{np-1} + B_{1n}^{1}\xi^{-np+1}\right)\cos\left[(np-1)\psi\right]\right.$$

$$+\left(C_{1n}^{1}\xi^{np-1}+D_{1n}^{1}\xi^{-np+1}\right)\sin\left[(np-1)\psi\right]$$

$$+\left(E_{1n}^{1}\xi^{np+1}+F_{1n}^{1}\xi^{-np-1}\right)\cos\left[(np+1)\psi\right]$$

$$+\left(G_{1n}^{1}\xi^{np+1}+H_{1n}^{1}\xi^{-np-1}\right)\sin\left[(np+1)\psi\right]\Big\} \tag{36}$$

$$\Phi_{2}^{(1)}(\xi,\psi)=\sum_{n=1,3,5\cdots}^{\infty}\Big\{\left(A_{2n}^{1}\xi^{np-1}+B_{2n}^{1}\xi^{-np+1}\right)\cos\left[(np-1)\psi\right]$$

$$+\left(C_{2n}^{1}\xi^{np-1}+D_{2n}^{1}\xi^{-np+1}\right)\sin\left[(np-1)\psi\right]$$

$$+\left(E_{2n}^{1}\xi^{np+1}+F_{2n}^{1}\xi^{-np-1}\right)\cos\left[(np+1)\psi\right]$$

$$+\left(G_{2n}^{1}\xi^{np+1}+H_{2n}^{1}\xi^{-np-1}\right)\sin\left[(np+1)\psi\right]\Big\} \tag{37}$$

The integral constants A_{1n}^{1}, B_{1n}^{1}, etc. and A_{2n}^{1}, B_{2n}^{1}, etc. are obtained from the boundary conditions in (28-31). The complete first-order solutions for the magnetic field regions in terms of the moving coordinates are derived for $np\neq 1$, which is a usual configuration in external rotor motors. Throughout this paper, only the air gap flux density distribution is calculated.

The flux density distribution in the air gap region is

$$B_{\xi,1}^{(1)}(\xi,\psi)=\sum_{n=1,3,5\cdots}^{\infty}-\mu_0\Big\{(np-1)\left(W_n\xi^{np-2}-X_n\xi^{-np}\right)\cos\left[(np-1)\psi-\omega t+\phi\right]$$

$$+(np+1)\left(Y_n\xi^{np}-Z_n\xi^{-np-2}\right)\cos\left[(np+1)\psi-\omega t-\phi\right]\Big\} \tag{38}$$

$$B_{\psi,1}^{(1)}(\xi,\psi)=\sum_{n=1,3,5\cdots}^{\infty}\mu_0\Big\{(np-1)\left(W_n\xi^{np-2}+X_n\xi^{-np}\right)\sin\left[(np-1)\psi-\omega t+\phi\right]$$

$$+(np+1)\left(Y_n\xi^{np}+Z_n\xi^{-np-2}\right)\sin\left[(np+1)\psi-\omega t-\phi\right]\Big\} \tag{39}$$

where the coefficients W_n, X_n, Y_n, and Z_n are given as follows

$$W_n = \frac{-npA_0 R_s^{2np-2}\left\{(1+\mu_r)R_m^{2np-2} - (1-\mu_r)R_r^{2np-2}\right\}}{(1+\mu_r)(R_r^{2np-2} - R_s^{2np-2})R_m^{2np-2} - (1-\mu_r)(R_m^{4np-4} - R_r^{2np-2}R_s^{2np-2})} \tag{40a}$$

$$X_n = \frac{-npA_0 R_m^{2np-2} R_s^{2np-2}\left\{(1-\mu_r)R_m^{2np-2} - (1+\mu_r)R_r^{2np-2}\right\}}{(1+\mu_r)(R_r^{2np-2} - R_s^{2np-2})R_m^{2np-2} - (1-\mu_r)(R_m^{4np-4} - R_r^{2np-2}R_s^{2np-2})} \tag{40b}$$

$$Y_n = \frac{-npA_0 R_s^{2np}\left\{(1+\mu_r)R_m^{2np+2} - (1-\mu_r)R_r^{2np+2}\right\}}{(1+\mu_r)(R_r^{2np+2} - R_s^{2np+2})R_m^{2np+2} - (1-\mu_r)(R_m^{4np+4} - R_r^{2np+2}R_s^{2np+2})} \tag{40c}$$

$$Z_n = \frac{-npA_0 R_m^{2np} R_s^{2np}\left\{(1-\mu_r)R_m^{2np+2} - (1+\mu_r)R_r^{2np+2}\right\}}{(1+\mu_r)(R_r^{2np+2} - R_s^{2np+2})R_m^{2np+2} - (1-\mu_r)(R_m^{4np+4} - R_r^{2np+2}R_s^{2np+2})} \tag{40d}$$

A_0 in the above equations is given by

$$A_0 = \frac{\mu_0 M_n}{\mu_r} \cdot \frac{R_m^{-(np-1)}}{(np)^2 - 1} \cdot \left\{ \frac{(np-1)R_m^{2np} + 2R_r^{np+1}R_m^{np-1} - (np+1)R_r^{2np}}{\frac{\mu_r+1}{\mu_r}\left[R_s^{2np} - R_r^{2np}\right] - \frac{\mu_r-1}{\mu_r}\left[R_m^{2np} - R_s^{2np}\left(R_r/R_m\right)^{2np}\right]} \right\} \tag{41}$$

E. Flux Density Distributions in the Moving Coordinates

Equations (38) and (39) describe the flux density distribution in the air gap region due to the rotor eccentricity in terms of the moving coordinates. These equations can provide information on the effects of the rotor eccentricity on the magnetic field. The total flux density distribution is the combination of the zero-order and first-order solutions

$$B_{\xi,1}(\xi,\psi,\varepsilon) = B_{\xi,1}^{(0)}(\xi,\psi) + \varepsilon B_{\xi,1}^{(1)}(\xi,\psi) + \cdots \tag{42}$$

$$B_{\psi,1}(\xi,\psi,\varepsilon) = B_{\psi,1}^{(0)}(\xi,\psi) + \varepsilon B_{\psi,1}^{(1)}(\xi,\psi) + \cdots \tag{43}$$

Therefore,

$$B_{\xi,1}(\xi,\psi,\varepsilon) = -\mu_0 \sum_{n=1,3,5\cdots}^{\infty} \left\{ npA_0\left(\xi^{np-1} + R_s^{2np}\xi^{-np-1}\right)\cos(np\psi) \right.$$

$$\left. + \varepsilon\left(np-1\right)\left(W_n\xi^{np-2} - X_n\xi^{-np}\right)\cos\left[(np-1)\psi - \omega t + \phi\right] \right.$$

$$+\varepsilon(np+1)\left(Y_n\xi^{np}-Z_n\xi^{-np-2}\right)\cos\left[(np+1)\psi+\omega t-\phi\right]\Big\} \tag{44}$$

$$B_{\psi,1}(\xi,\psi,\varepsilon)=\mu_0\sum_{n=1,3,5\cdots}^{\infty}\Big\{npA_0\left(\xi^{np-1}-R_s^{2np}\xi^{-np-1}\right)\sin(np\psi)$$

$$+\varepsilon\left(np-1\right)\left(W_n\xi^{np-2}+X_n\xi^{-np}\right)\sin\left[(np-1)\psi-\omega t+\phi\right]$$

$$+\varepsilon(np+1)\left(Y_n\xi^{np}+Z_n\xi^{-np-2}\right)\sin\left[(np+1)\psi+\omega t-\phi\right]\Big\} \tag{45}$$

Equations (44) and (45) are complete solutions for the flux density distribution of the air gap in terms of the coordinates that originate from the rotor reference coordinate system.

F. Flux Density Distributions in the Fixed Coordinate System

Equations (44) and (45) are not in a convenient form for the purpose of other applications. It is therefore reasonable to represent them in terms of fixed coordinates. It is well known that in a quasi-static magnetic field as considered in the present paper, the field variables which are evaluated in different reference coordinate systems, are the same whether viewed from one coordinate system or the other [10]. In the present paper, it follows that

$$\vec{\bar{H}}(r,\theta,\varepsilon)=\vec{H}(\xi,\psi,\varepsilon) \tag{46}$$

$$\vec{\bar{M}}(r,\theta,\varepsilon)=\vec{M}(\xi,\psi,\varepsilon) \tag{47}$$

$$\vec{\bar{B}}(r,\theta,\varepsilon)=\vec{B}(\xi,\psi,\varepsilon) \tag{48}$$

and consequently

$$\bar{\Psi}(r,\theta,\varepsilon)=\Phi(\xi,\psi,\varepsilon) \tag{49}$$

where the magnetic field vectors with a bar indicate the field variables described by the fixed coordinates and in the same context, $\bar{\Psi}$ is the magnetic potential expressed by the

fixed coordinates. The flux density distribution in the fixed coordinate system can be obtained directly by substituting the coordinate transformations (3a,b) into the equation (48). However, note that the flux density distribution is expressed in a vector form and the vector bases are taken with respect to the coordinates of each reference frame. Accordingly, the vector components can not be directly compared with each other. The following procedure is, therefore, suggested.

The flux density in the fixed coordinate system is defined as

$$\overline{B}_r = -\mu_0 \frac{\partial \Psi}{\partial r} \tag{50}$$

$$\overline{B}_\theta = -\mu_0 \frac{1}{r} \frac{\partial \Psi}{\partial \theta} \tag{51}$$

By equation (49) and the coordinate transform equation (3a,b) as well as their derivatives with respect to the fixed coordinates, the above equations can be evaluated as follows.

$$\overline{B}_r = -\mu_0 \left(\frac{\partial \Phi}{\partial \xi} \frac{\partial \xi}{\partial r} + \frac{\partial \Phi}{\partial \psi} \frac{\partial \psi}{\partial r} \right) \tag{52}$$

$$\overline{B}_\theta = -\frac{\mu_0}{r} \left(\frac{\partial \Phi}{\partial \xi} \frac{\partial \xi}{\partial \theta} + \frac{\partial \Phi}{\partial \psi} \frac{\partial \psi}{\partial \theta} \right) \tag{53}$$

Then the air gap flux density distributions can be explicitly represented by using the perturbation equations (20a,b), i.e.,

$$\overline{B}_r = -\mu_0 \frac{\partial \Phi^{(0)}}{\partial \xi} - \varepsilon \mu_0 \left\{ \frac{\partial \Phi^{(1)}}{\partial \xi} - \frac{1}{r^2} \frac{\partial \Phi^{(0)}}{\partial \psi} \sin(\theta - \phi) \right\} \tag{54}$$

$$\overline{B}_\theta = -\frac{\mu_0}{r} \frac{\partial \Phi^{(0)}}{\partial \psi} - \varepsilon \mu_0 \left\{ \frac{1}{r} \frac{\partial \Phi^{(1)}}{\partial \psi} + \frac{1}{r} \frac{\partial \Phi^{(0)}}{\partial \xi} \sin(\theta - \phi) + \frac{1}{r^2} \frac{\partial \Phi^{(0)}}{\partial \psi} \cos(\theta - \phi) \right\} \tag{55}$$

Now, combining the coordinate transformation equations (3a,b) with (44) and (45) as well as Taylor series expansions up to the first order of ε gives the desired solutions in the fixed coordinate system.

$$\overline{B}_r(r,\theta)=\sum_{n=1,3,5\cdots}^{\infty}(np)A_0\left(r^{np-1}+R_s{}^{2np}r^{-np-1}\right)\cos[np(\theta-\omega t)+\varepsilon\frac{np}{r}\sin(\theta-\phi)]$$

$$+\varepsilon\left[\sum_{n=1,3,5\cdots}^{\infty}(np)\frac{A_0}{2}\left\{(2-np)r^{np-2}+npR_s^{2np}r^{-np-2}\right\}\right.$$

$$\cdot\cos[(np-1)\theta-np\omega t+\phi+\varepsilon\frac{np}{r}\sin(\theta-\phi)]$$

$$+\sum_{n=1,3,5\cdots}^{\infty}(np)\frac{A_0}{2}\left\{-npr^{np-2}+(np+2)R_s^{2np}r^{-np-2}\right\}$$

$$\cdot\cos[(np+1)\theta-np\omega t-\phi+\varepsilon\frac{np}{r}\sin(\theta-\phi)]$$

$$-\sum_{n=1,3,5\cdots}^{\infty}\mu_0(np-1)\left(W_nr^{np-2}-X_nr^{-np}\right)$$

$$\cdot\cos[(np-1)\theta-np\omega t+\phi+\varepsilon\frac{(np-1)}{r}\sin(\theta-\phi)]$$

$$-\sum_{n=1,3,5\cdots}^{\infty}\mu_0(np+1)\left(Y_nr^{np}-Z_nr^{-np-2}\right)$$

$$\left.\cdot\cos[(np+1)\theta-np\omega t-\phi+\varepsilon\frac{(np+1)}{r}\sin(\theta-\phi)]\right] \qquad (56)$$

$$\overline{B}_\theta(r,\theta)=\sum_{n=1,3,5\cdots}^{\infty}-(np)A_0\left(r^{np-1}-R_s{}^{2np}r^{-np}\right)\sin[np(\theta-\omega t)+\varepsilon\frac{np}{r}\sin(\theta-\phi)]$$

$$+\varepsilon\left[\sum_{n=1,3,5\cdots}^{\infty}(np)\frac{A_0}{2}\left\{(np-2)r^{np-2}+npR_s^{2np}r^{-np-2}\right\}\right.$$

$$\cdot\sin[(np-1)\theta-np\omega t+\phi+\varepsilon\frac{np}{r}\sin(\theta-\phi)]$$

$$+\sum_{n=1,3,5\cdots}^{\infty}(np)\frac{A_0}{2}\left\{npr^{np-2}+(np+2)R_s^{2np}r^{-np-2}\right\}$$

$$\cdot\sin[(np+1)\theta-np\omega t-\phi+\varepsilon\frac{np}{r}\sin(\theta-\phi)]$$

$$+\sum_{n=1,3,5\cdots}^{\infty}\mu_0(np-1)\left(W_n r^{np-2}+X_n r^{-np}\right)$$

$$\cdot\sin[(np-1)\theta-np\omega t+\phi+\varepsilon\frac{(np-1)}{r}\sin(\theta-\phi)]$$

$$+\sum_{n=1,3,5\cdots}^{\infty}\mu_0(np+1)\left(Y_n r^{np}+Z_n r^{-np-2}\right)$$

$$\cdot\sin[(np+1)\theta-np\omega t-\phi+\varepsilon\frac{(np+1)}{r}\sin(\theta-\phi)]\Big] \qquad (57)$$

Equations (56) and (57) are the most complete solutions for the flux density distribution in the air gap region due to the rotor eccentricity in the fixed coordinate system, but can be simplified by neglecting the perturbed phase terms in the solutions as follows.

$$\overline{B}_r(r,\theta)=\sum_{n=1,3,5\cdots}^{\infty}(np)A_0\left(r^{np-1}+R_s{}^{2np}r^{-np-1}\right)\cos[np(\theta-\omega t)]$$

$$+\varepsilon\sum_{n=1,3,5\cdots}^{\infty}\left(np\frac{A_0}{2}\left\{(2-np)r^{np-2}+npR_s^{2np}r^{-np-2}\right\}-\mu_0(np-1)\left(W_n r^{np-2}-X_n r^{-np}\right)\right)$$

$$\cdot\cos[(np-1)\theta-np\omega t+\phi]$$

$$+\varepsilon\sum_{n=1,3,5\cdots}^{\infty}\left(np\frac{A_0}{2}\left\{-npr^{np-2}+(np+2)R_s^{2np}r^{-np-2}\right\}-\mu_0(np+1)\left(Y_n r^{np-2}-Z_n r^{-np}\right)\right)$$

$$\cdot\cos\left[(np+1)\theta-np\omega t-\phi\right] \qquad (58)$$

$$\overline{B}_\theta(r,\theta)=\sum_{n=1,3,5\cdots}^{\infty}(np)A_0\left(r^{np-1}-R_s{}^{2np}r^{-np-1}\right)\sin[np(\theta-\omega t)]$$

$$+\varepsilon\sum_{n=1,3,5\cdots}^{\infty}\left(np\frac{A_0}{2}\left\{(np-2)r^{np-2}+npR_s^{2np}r^{-np-2}\right\}+\mu_0(np-1)\left(W_n r^{np-2}+X_n r^{-np}\right)\right)$$

$$\cdot \sin[(np-1)\theta - np\omega t + \phi]$$

$$+ \varepsilon \sum_{n=1,3,5\cdots}^{\infty} \left(np \frac{A_0}{2} \left\{ npr^{np-2} + (np+2) R_s^{2np} r^{-np-2} \right\} + \mu_0 (np+1) \left(Y_n r^{np} + Z_n r^{-np-2} \right) \right)$$

$$\cdot \sin\left[(np+1)\theta - np\omega t - \phi\right] \qquad (59)$$

These simplified solutions (58) and (59) yield few errors in numerical values when compared with the results from the finite element analyses. However, they are expressed in forms that are more convenient for other applications. Note that the original unperturbed flux density distribution is recovered when ε=0.

III. COMPARISON OF THE PERTURBATION AND FINITE ELEMENT SOLUTIONS

The perturbation solutions of the eccentric magnetic field have been verified for a prototype motor by finite element calculations. The geometric parameters of the motor are given in Table 1 in Appendix 2. The finite element model of the motor to be analyzed was built through a magnetic finite element analysis package, TOSCA with a pre- and post-processor called OPERA. The analysis was executed with the linear magnetic material properties of the stator iron and the rotor magnets. Unlike the perturbation model in which the relative permeability of the stator iron is considered infinite, the finite element model considers the relative permeability of the stator iron finite, i.e., μ_r=1364. For this reason, the boundary conditions of the finite element model are approximated by the far field conditions, where the scalar potentials are zero. The finite element model was built on the moving coordinate system due to a relative simplicity of expressing the rotor magnet

directions. Therefore the results are to be compared with those from equations (44) and (45).

Fig. 3 shows the flux density distributions in the radial direction calculated by the perturbation and the finite element analysis for the case of 10% eccentricity at an instant of $\phi=0^o$ and $\omega t=0^o$. The figure shows the flux density curves in the range only from 0^o to 180^o since they are symmetric about 180^o for $\phi=0^o$ and $\omega t=0^o$. The figure shows the flux density from both calculations are in good agreement in amplitude and wave form. Fig. 4 compares the flux density distributions in the radial direction for the case of 50% eccentricity at an instant of $\phi=45^o$ and $\omega t=30^o$. Again, the distributions show good agreement despite the relatively large eccentricity, which shows the effectiveness of the perturbation method for calculation of eccentric magnetic field problems. Fig. 5 reveals the eccentric field effect on the flux density distribution in the radial direction, $B_{\xi}^{(1)}$, by various rotor eccentricities. Note that the additional flux density has complicated profiles and sharp peaks also appear on the flux density distribution curves, which may yield additional unwanted effects on motor performance. Fig. 6 and Fig. 7 show the flux density distributions in the radial and circumferential directions along an imaginary circle in the air gap region with the radius of $R_s+0.2g$ from the center of the stator. Again the results show good agreement except for the error in the magnitude of some peaks in the circumferential direction but this minor discrepancy may be yielded by errors in the finite element model discretization. All the perturbation solutions contain only the linear terms up to the first order of ε and clearly can be improved by taking more terms.

IV. CONCLUSION

A complete procedure of analysis for predicting the instantaneous magnetic field distribution in the air gap region of permanent magnet motors with the rotor eccentricity is developed. The governing field equations and the associated boundary conditions are formulated and solved by the aid of a perturbation method, which is introduced to treat the nonlinear boundary conditions caused by the rotor eccentricity. The perturbation analysis is validated by the corresponding finite element analysis. Only the linear terms up to the first order solutions are sufficient for obtaining good results compared with the finite element analysis. Comprehensive understanding of the magnetic field induced by the rotor eccentricity will help to develop motors with better design and performance.

ACKNOWLEDGMENTS

The authors gratefully acknowledge Dr. Sangmoon Hwang of Pusan National University in Korea for the help of the finite element calculation and also the University of California Computer Mechanics Laboratory for its support of this work.

REFERENCES

[1] N. Schirle and D.K. Lieu, “History and trends in the development of motorized spindles for hard disk drives,” *IEEE Trans. on Magnetics*, Vol. 32, No. 3, 1996, pp.1703-1708.

[2] S. A. Swan, “Effect of rotor eccentricity on the magnet field in air gap of a nonsalient pole machine,” *Proc. IEE* Vol. 110, No. 5, 1963, pp.903-905.

[3] R. Belmans, W. Geysen, H. Jordan, and A. Vandenput, " Unbalanced magnet pull in three phase two pole induction motor with eccentric rotor," *IEE Conference Publication* No. 213, 1982, pp.65-69.

[4] R. Belmans, A. Vandenput, and W. Geysen, " Influenced of unbalanced magnetic pull on the radial stability of flexible shaft induction machines," *IEE Proc*. Vol. 134, Pt. B, No. 2, March 1987, pp. 101-109.

[5] R. Cameron, W. T. Thomson, and A. B. Dow, "Vibration and current monitoring for detecting air gap eccentricity in large induction motors," *IEE Proc*. Vol. 133, Pt. B, No.3, May 1986, pp. 155-163.

[6] G. Dorrell, W. T. Thomson, and S. Roach, " Combined effects of static and dynamic eccentricity on air gap flux waves and the application of current monitoring to detect dynamic eccentricity in 3-phase induction machines," *IEE Conference Publication* No. 412, Electrical machines and drives, Sept. 1995, pp. 151-155.

[7] Q. Zhu and D. Howe, "Electromagnetic noise radiated by brushless permanent magnet dc drives." *Source unknown*.

[8] Chao, Z. J. Liu and T. S. Low, "Unbalanced magnet pull in PM synchronous machines-Its relation with stator teeth and armature winding," *Proceedings of incremental motion control systems and devices*. 1996, pp.79-84.

[9] C-W Lee, *Vibration Analysis of Rotors*, Kluwer Academic Publishers, 1993.

[10] J. R. Melcher, *Continuum electromechanics*, The MIT Press, 1981.

[11]Q. Zhu, D. Howe, E. Bolte, and B. Ackermann, "Instantaneous magnetic field distribution in brushless permanent magnet DC motors, Part I : Open-circuit field," *IEEE Trans. on Magnetics*, Vol. 29, No. 1, Jan. 1993, pp.124-135.

[12]B. Hague, *Electromagnetic Problems in Electrical Engineering*, Oxford University Press. London, 1929.

[13]A. Nayfeh, *Perturbation Methods*, John Wiley & Sons, 1973.

APPENDIX 1 : Derivation of Coordinate Transformation Equations (3a, b)

Consider the coordinate relationship detailed in Fig. 2 in the domain of the air gap or the magnet pole region. In the figure, let *P* be a point defined by the polar coordinates *r* and θ with respect to the origin O_s in the fixed coordinate system. It is necessary to be able to express ξ and ψ as a Fourier series of *r* and θ.

By drawing the perpendicular line from O_s upon the line P-O_r the following expression is produced.

$$\varepsilon \sin(\psi + \omega t - \phi) = r \sin(\psi + \omega t - \theta)$$

or

$$\varepsilon\left\{e^{j(\psi+\omega t-\phi)} - e^{-j(\psi+\omega t-\phi)}\right\} = r\left\{e^{j(\psi+\omega t-\theta)} - e^{-j(\psi+\omega t-\theta)}\right\}$$

where $j = \sqrt{-1}$

Rewriting the above equation yields

$$\left\{\varepsilon e^{j(\omega t-\phi)} - re^{j(\omega t-\theta)}\right\}e^{j\psi} = \left\{\varepsilon e^{-j(\omega t-\phi)} - re^{-j(\omega t-\theta)}\right\}e^{-j\psi}$$

or simply

$$e^{j2\psi} = \frac{\varepsilon e^{-j(\omega t-\phi)} - er^{-j(\omega t-\theta)}}{\varepsilon e^{j(\omega t-\phi)} - er^{j(\omega t-\theta)}} = \frac{e^{-j(\omega t-\phi)}\{re^{j(\theta-\phi)} - \varepsilon\}}{e^{j(\omega t-\phi)}\{re^{-j(\theta-\phi)} - \varepsilon\}}$$

Taking logarithms on both side of the above equation yields

$$j2\psi = -j2(\omega t - \phi) + \log\{re^{j(\theta-\phi)} - \varepsilon\} - \log\{re^{-j(\theta-\phi)} - \varepsilon\}$$

The right hand side can be expanded in a convergent series. With $r > \varepsilon$ for most permanent magnet motors, the above equation is expressed as

$$j2\psi = -j2(\omega t - \phi) + \log[re^{j(\theta-\phi)}\{1-\frac{\varepsilon}{r}e^{-j(\theta-\phi)}\}] - \log[re^{-j(\theta-\phi)}\{1-\frac{\varepsilon}{r}e^{j(\theta-\phi)}\}]$$

$$= -j2(\omega t - \phi) + j2(\theta - \phi) + \log\{1-\frac{\varepsilon}{r}e^{-j(\theta-\phi)}\} - \log\{1-\frac{\varepsilon}{r}e^{j(\theta-\phi)}\}$$

Since $\frac{\varepsilon}{r}e^{\pm j(\theta-\phi)}$ has a modulus less than unity the right hand side can be again expanded into a convergent series.

$$j2\psi = j2(\theta - \omega t) + \frac{\varepsilon}{r}\{e^{j(\theta-\phi)} - e^{-j(\theta-\phi)}\} + \cdots + \frac{1}{n}\frac{\varepsilon^n}{r^n}\{e^{jn(\theta-\phi)} - e^{-jn(\theta-\phi)}\} + \cdots$$

or

$$\psi = \theta - \omega t + \sum_{n=1}^{\infty}\frac{1}{n}\frac{\varepsilon^n}{r^n}\sin[n(\theta-\phi)]$$

The terms up to the first order of ε are retained for the perturbation analysis.

$$\psi = \theta - \omega t + \frac{\varepsilon}{r}\sin(\theta-\phi) + O(\varepsilon^2)$$

And ξ is obtained by applying the cosine law.

$$\xi = \sqrt{r^2 + \varepsilon^2 - 2r\varepsilon\cos(\theta-\phi)}$$

Taking a Taylor expansion of the right hand side gives the following expression.

$$\xi = r - \varepsilon\cos(\theta-\phi) + O(\varepsilon^2)$$

APPENDIX 2 : Geometric Parameters of the Model Motor

Table 1 : Geometric parameters of the model motor

Parameter	Symbol	Value (unit)
Pole number	$2p$	8
Pole-arc/pole-pitch ratio	α_p	1.0
Air gap length	g	0.25 (mm)
Radial thickness of magnets	h_m	0.80 (mm)
Stator radius	R_s	10.64 (mm)
Magnet remanence	B_r	0.71 (T)
Relative permeability	μ_r	1.26

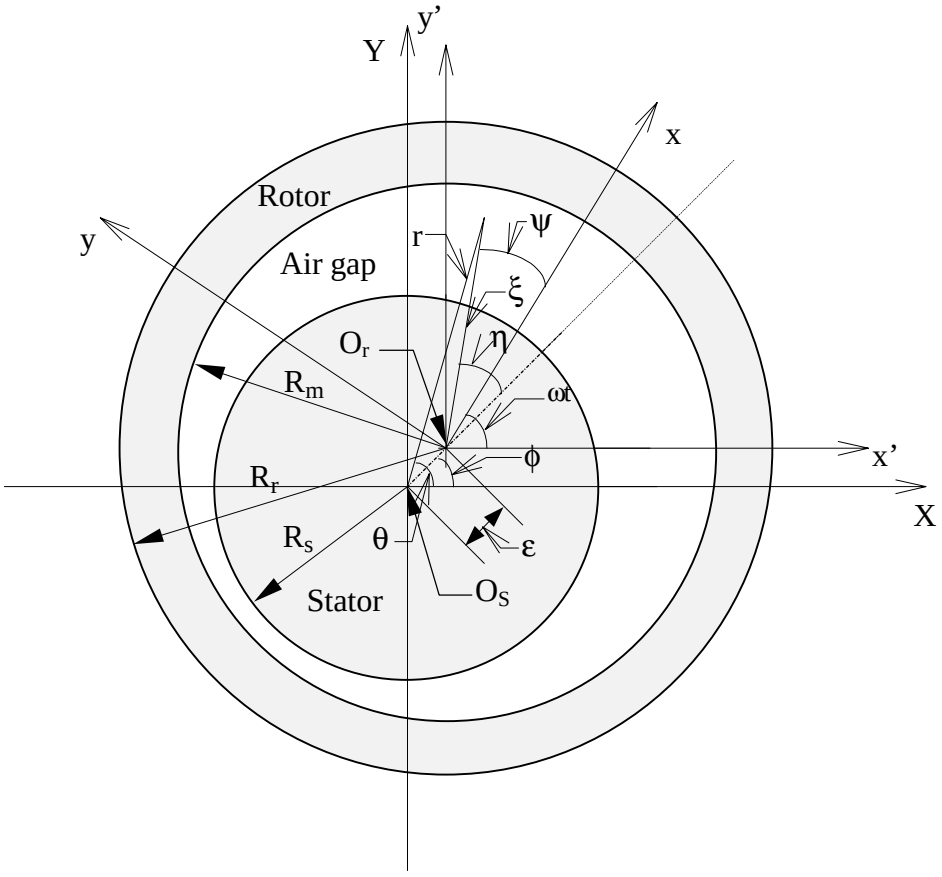

Fig. 1. Geometric configuration of the model motor
(Air gap is exaggerated for clarity)

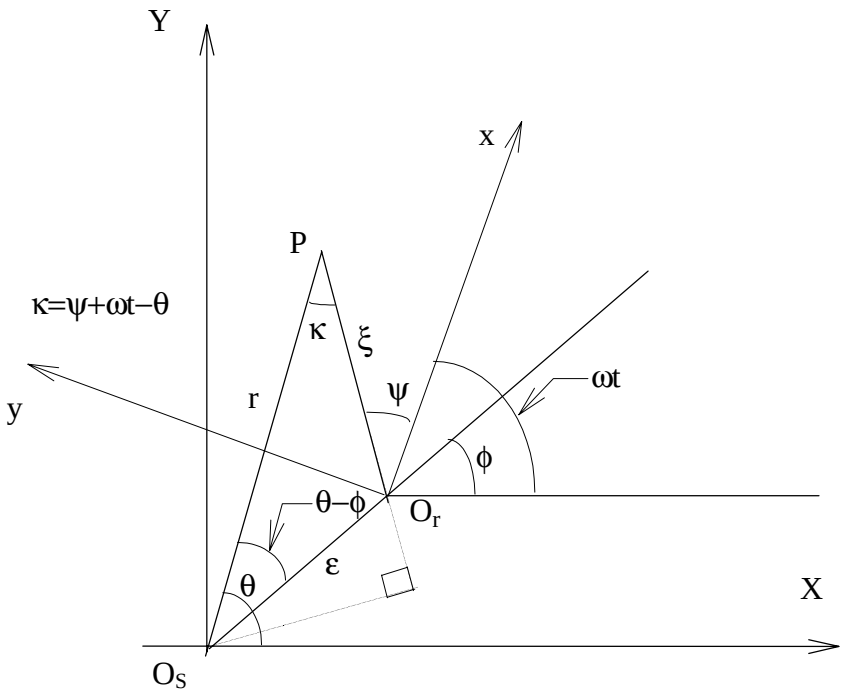

Fig.2. Coordinate relationship of the fixed and moving coordinates

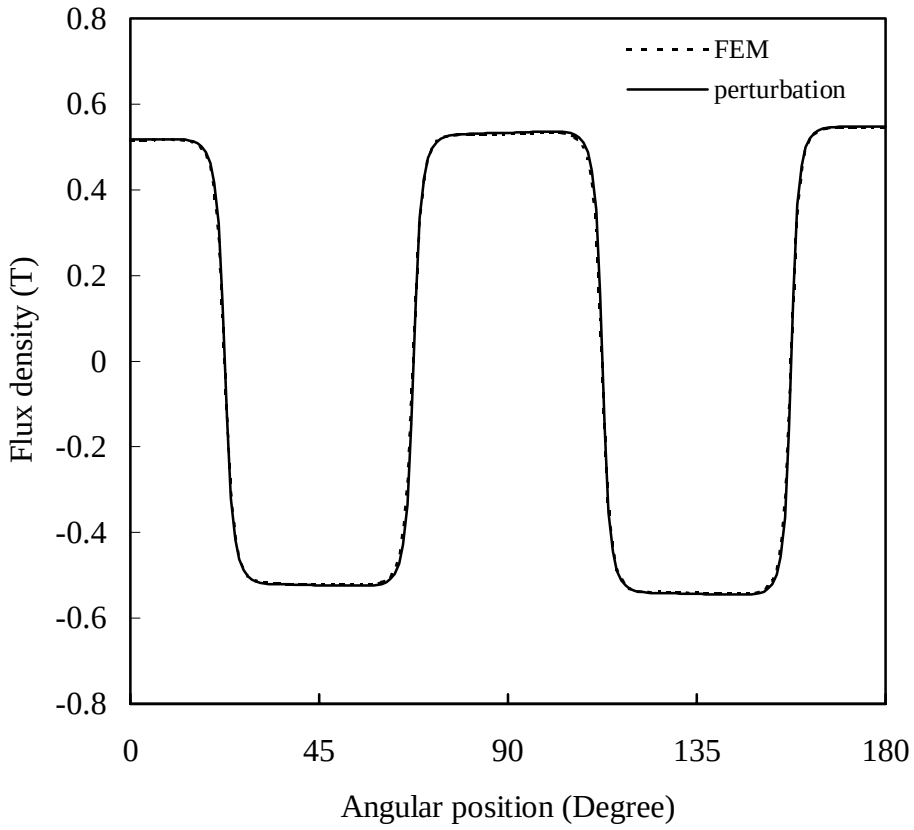

Fig. 3. Flux density distributions along the surface of the stator calculated by the perturbation and FEM for 10% eccentricity at an instant of $\phi=0^o$ and $\omega t=0^o$

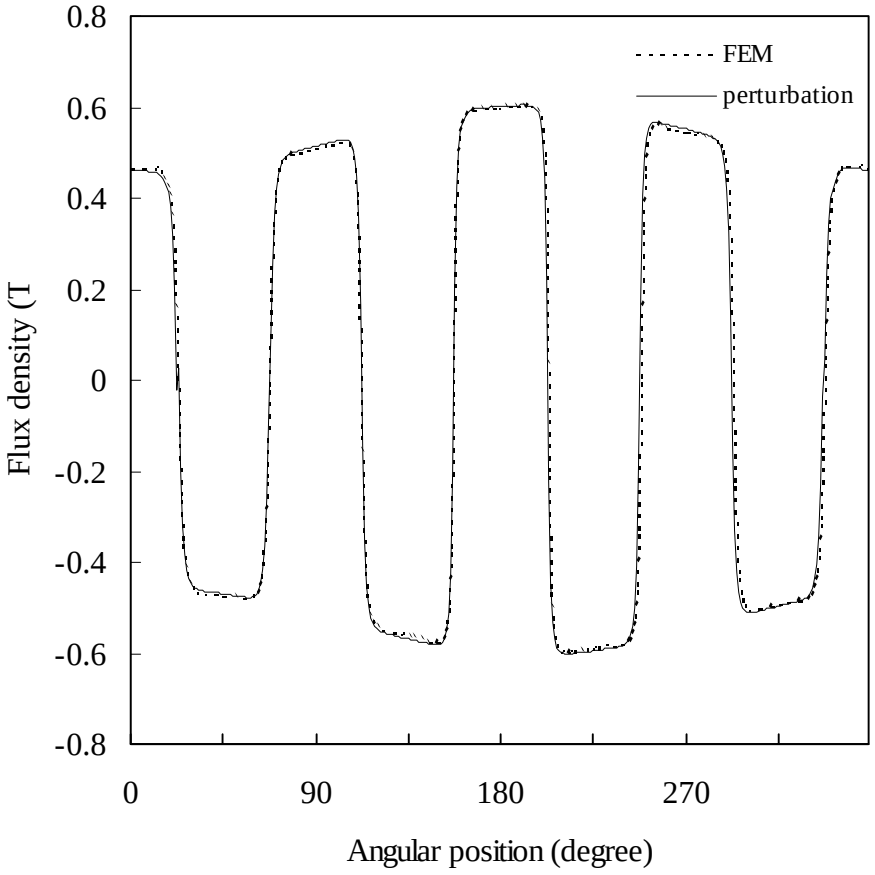

Fig. 4. Flux density distributions along the surface of the stator for 50% eccentricity at an instant of $\phi=45^{o}$ and $\omega t=30^{o}$.

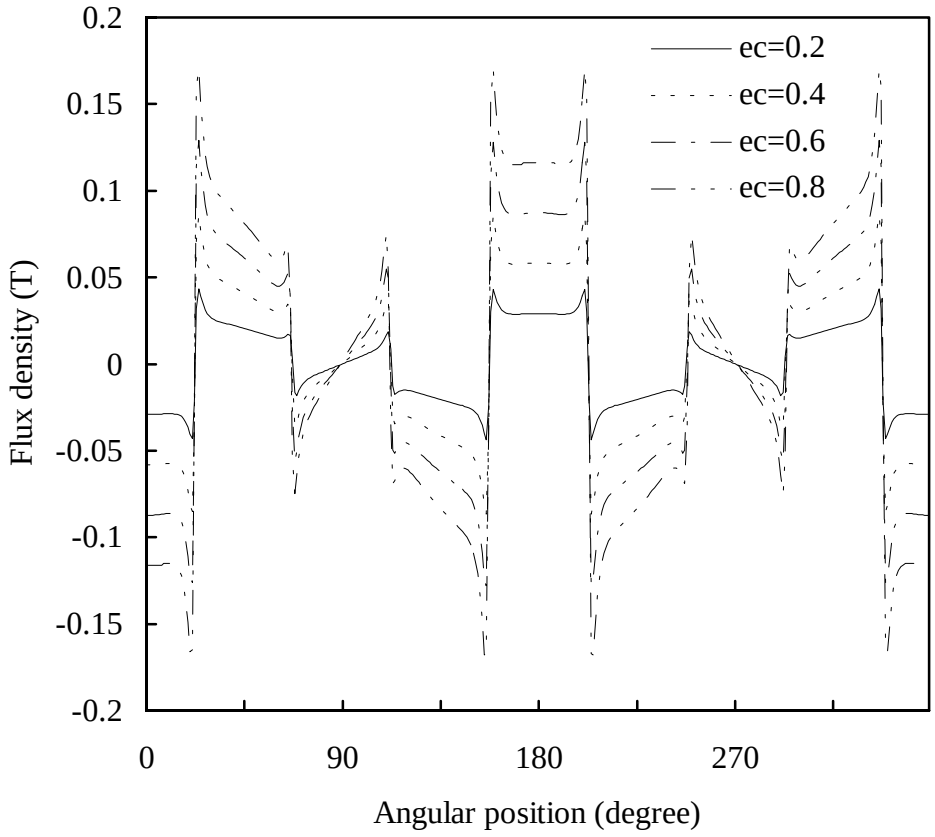

Fig. 5. Additional flux density distributions along the surface of the stator at an instant of $\phi=0^o$ and $\omega t=0^o$.

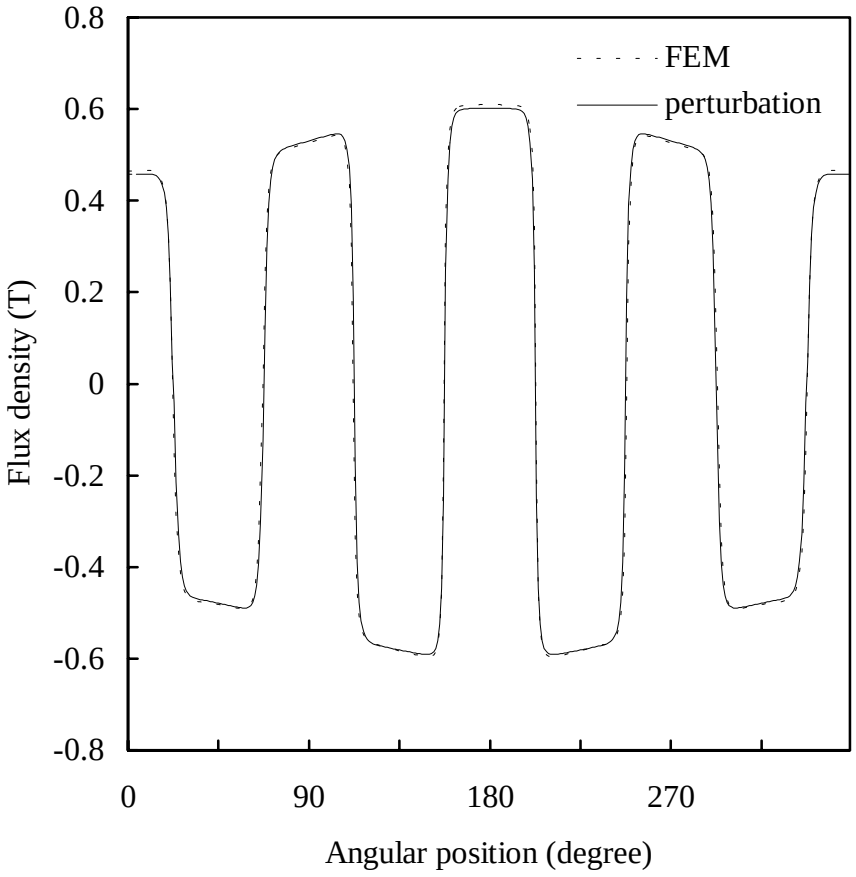

Fig. 6. Flux density distributions of the radial direction in the air gap region (R_S+0.2g) for 50% eccentricity at an instant of $\phi=0^o$ and $\omega t=0^o$.

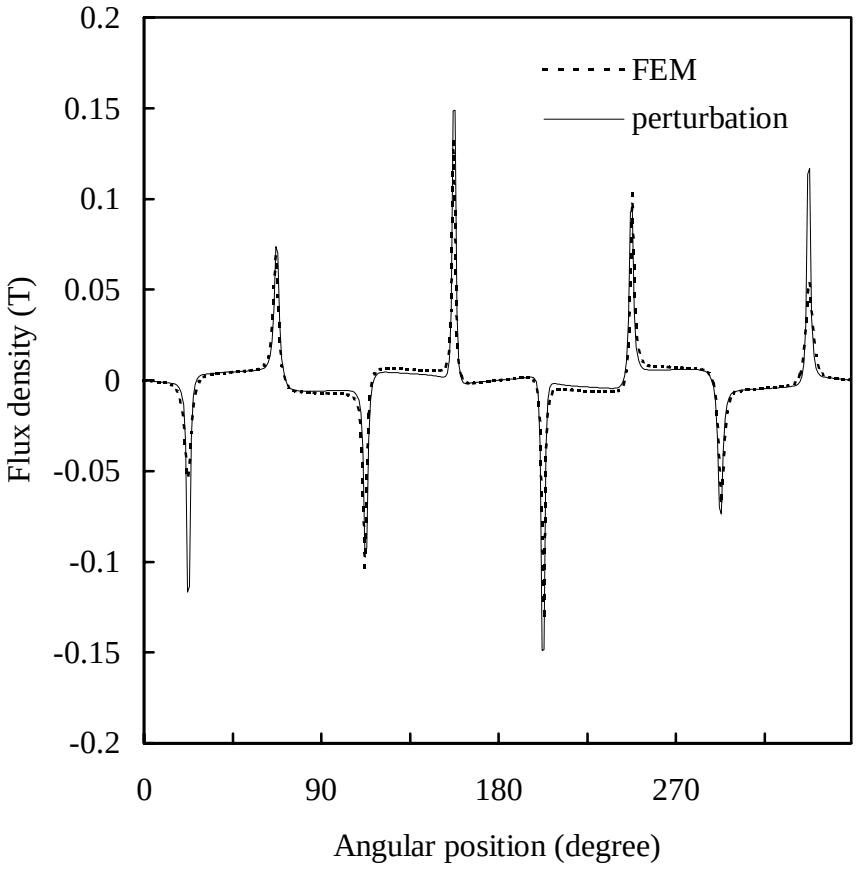

Fig. 7. Flux density distributions of the circumferential direction in the air gap region (R_S+0.2g) for 50% eccentricity at an instant of $\phi=0^o$ and $\omega t=0^o$.